ACSNANO

www.acsnano.org

3D Flexible, Conductive, and Recyclable $Ti_3C_2T_x$ MXene-Melamine Foam for High-Areal-Capacity and Long-Lifetime Alkali-Metal Anode

Haodong Shi,[‖] Meng Yue,[‖] Chuanfang John Zhang,[‖] Yanfeng Dong, Pengfei Lu, Shuanghao Zheng, Huijuan Huang, Jie Chen, Pengchao Wen, Zhaochao Xu, Qiong Zheng,* Xianfeng Li, Yan Yu,* and Zhong-Shuai Wu*

Cite This: *ACS Nano* 2020, 14, 8678−8688

Read Online

ACCESS | Metrics & More | Article Recommendations | Supporting Information

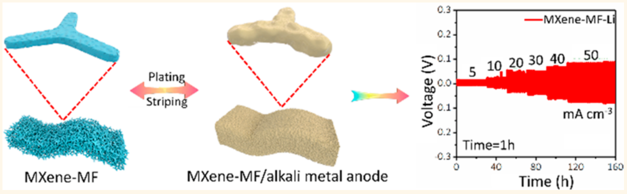

ABSTRACT: **Alkali metals are ideal anodes for high-energy-density rechargeable batteries, while seriously hampered by limited cycle life and low areal capacities. To this end, rationally designed frameworks for dendrite-free and volume-changeless alkali-metal deposition at both high current densities and capacities are urgently required. Herein, a general 3D conductive $Ti_3C_2T_X$ MXene-melamine foam (MXene-MF) is demonstrated as an elastic scaffold for dendrite-free, high-areal-capacity alkali anodes (Li, Na, K). Owing to the lithiophilic nature of F-terminated MXene, conductive macroporous network, and excellent mechanical toughness, the constructed MXene-MF synchronously achieves a high current density of 50 mA cm^{-2} for Li plating, high areal capacity (50 mAh cm^{-2}) with high Coulombic efficiency (99%), and long lifetime (3800 h), surpassing the Li anodes reported recently. Meanwhile, MXene-MF shows flat voltage profiles for 720 h at 10 mA cm^{-2} for the Na anode and 800 h at 5 mA cm^{-2} for the K anode, indicative of the wide applicability. Notably, the high current density of 20 mA cm^{-2} for 20 mAh cm^{-2} for the Na anode, accompanying good recyclability was rarely achieved before. When coupled with sulfur or $Na_3V_2(PO_4)_3$ cathodes, the assembled MXene-MF alkali (Li, Na)-based full batteries showcase enhanced rate capability and cycling stability, demonstrating the potential of MXene-MF for advanced alkali-metal batteries.**

KEYWORDS: *alkali-metal anode, 3D framework, MXene, high areal capacity, dendrite-free*

The increasing popularity of hybrid electric vehicles and portable electronics demands high-energy-density batteries.[1−3] Among numerous anode candidates, alkali-metal anodes are considered as ideal ones due to their high theoretical capacities (lithium (Li): 3680 mAh g^{-1}, sodium (Na): 1165 mAh g^{-1}, and potassium (K): 687 mAh g^{-1}) and low redox potential (Li: −3.04 V, Na: −2.71 V, and K: −2.93 V *vs* SHE).[4−7] Besides, when paired with high-capacity cathodes such as oxygen (O_2) and sulfur (S), high-energy-density batteries can be achieved for next-generation electronics.[8−12] Unfortunately, the undesirable growth of dendrites and the infinite relative change of volume during cycling processes have blocked the commercialization of alkali-metal anodes.[13−16]

Until now, tremendous efforts have been processed to resolve the aforementioned issues, such as optimizing the electrolyte formulation and functional additives (*e.g.*, $LiNO_3$, Cs^+, Na_2S_6),[17−20] employing the solid-state electrolyte (*e.g.*, $Li_{0.34}La_{0.56}TiO_3$, $Li_{6.5}La_3Zr_{1.5}Ta_{0.5}O_{12}$, $Li_7La_{2.75}Ca_{0.25}Zr_{1.75}Nb_{0.25}O_{12}$),[21,22] and engineering alkali-metal-based alloys (*e.g.*, Li−Zn, Li−Si, Na−Sn).[23−25] Nevertheless, issues such as the huge volume changes and inhomogeneous ion flux distribution on copper (Cu) or alkali-metal foil, especially at high current densities (≥10 mA cm^{-2}) and deposition capacities (≥10 mAh cm^{-2}), are yet to be solved. To this end, three-dimensional (3D) porous and conductive scaffolds,[26,27] *e.g.*, porous Cu,[28] nickel foam,[29] carbon nanotube sponges,[30] and a graphene-based aerogel,[31,32]

Received: April 10, 2020
Accepted: June 12, 2020
Published: June 12, 2020

ACS Publications

https://dx.doi.org/10.1021/acsnano.0c03042

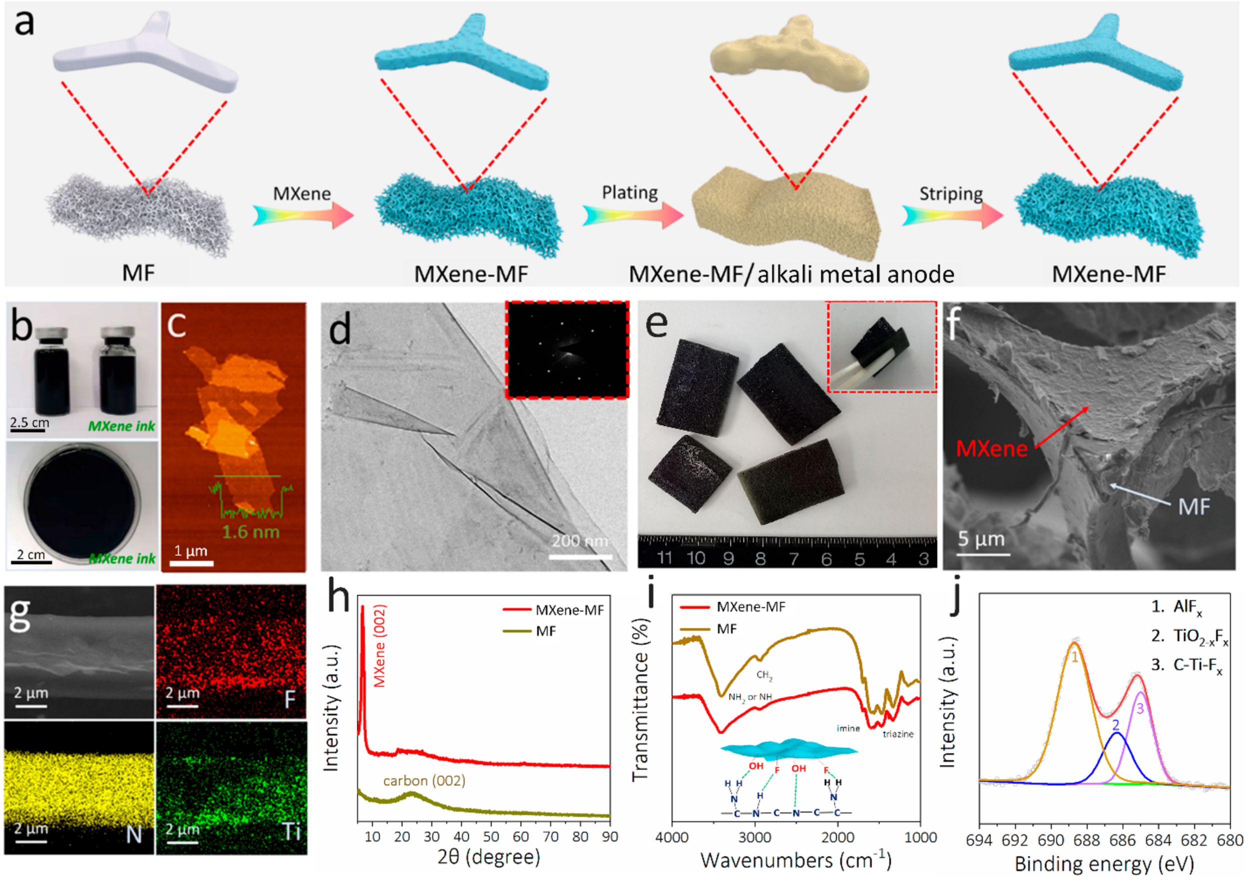

Figure 1. Fabrication and characterization of 3D MXene-MF scaffolds. (a) Schematic illustration of the fabrication process of the 3D MXene-MF for the alkali-metal anode. (b) Photographs of the MXene ink. (c) AFM image and height profile of MXene nanosheets. (d) TEM image of MXene nanosheets. Inset is the corresponding SAED image. (e) Photographs of MXene-MF. Inset is the corresponding image under a bending state. (f) SEM image and (g) EDS elemental mapping of fluorine (red), nitrogen (yellow), and titanium (green) of MXene-MF. (h) XRD patterns and (i) FTIR spectra of MXene-MF and bare MF. (j) High-resolution F 1s XPS spectrum of MXene-MF.

are proposed to effectively regulate the alkali-metal ion flux, suppress the dendrite growth, and minimize the volume change of the alkali anode. However, those scaffolds suffer from heavy mass density or poor mechanical toughness, resulting in limited capacity and decreased energy density. Recently, MXenes are rising as an emerging of two-dimensional (2D) transition metal carbides or carbonitrides. Typically, 2D titanium carbide ($Ti_3C_2T_x$, where T_x represents the surface groups) possesses high electronic conductivity (~10^4 S cm^{-1})[33−35] and inherent lithiophilic surface terminations (O, F, OH, Cl), making it an ideal building block material for 3D porous scaffolds for depositing alkali-metal deposition.[36−38] Unfortunately, conventional freestanding MXene films with densely compacted nanosheets offer a limited space against increased capacity of alkali metals, which fails to efficiently withstand their large volume stress from the latter during the stripping and plating process.[39] That is to say, designing a 3D lightweight, flexible, conductive MXene scaffold with high mechanical strength capability with synchronously realizing high current density and large capacity is an urgent need for alkali-metal anodes.

In this work, we propose a general cost-effective, scalable strategy of constructing a recyclable, flexible, and conductive 3D MXene-MF, *via* soaking a commercial polymer melamine foam (MF) in MXene ink by strong affinity of hydrogen bonding, for dendrite-free, stable, high-capacity alkali-metal anodes. By taking advantages of the high conductivity and lithiophilic surfaces from MXene, in combination with the porous, lightweight, and flexible nature from 3D MF, the resulting MXene-MF possesses a 3D interconnected porous conductive network with good mechanical flexibility and strength, enabling a highly dense and homogeneous alkali-metal deposition and suppressing volume fluctuation at both high current density and deposition capacity. Consequently, a high current density of 50 mA cm^{-2} for 50 mAh cm^{-2} and a long cycling life up to 3800 h are simultaneously achieved for the Li anode, Meanwhile, a high areal deposition capacity of 20 mAh cm^{-2} for the Na anode and 5 mAh cm^{-2} for the K anode are also realized. Moreover, such a robust 3D architecture guarantees repeated cycling without decomposing the structural integrity. By pairing MXene-MF-Li with sulfur (S) and MXene-MF-Na with $Na_3V_2(PO4)_3$ (NVP), respectively, the assembled full batteries showcase improved cycling and rate performance, demonstrative of the potential of MXene-MF in constructing high-energy-density batteries.

RESULTS AND DISCUSSION

The fabrication process of MXene-MF for alkali-metal anode (Li, Na, K) is schematically illustrated in Figure 1a. First, a commercial flexible MF with interconnected continuously macroporous structure (30−130 μm, Figure S1) was soaked in highly concentrated MXene ink (10 mg mL^{-1}, 3600 S cm^{-1},

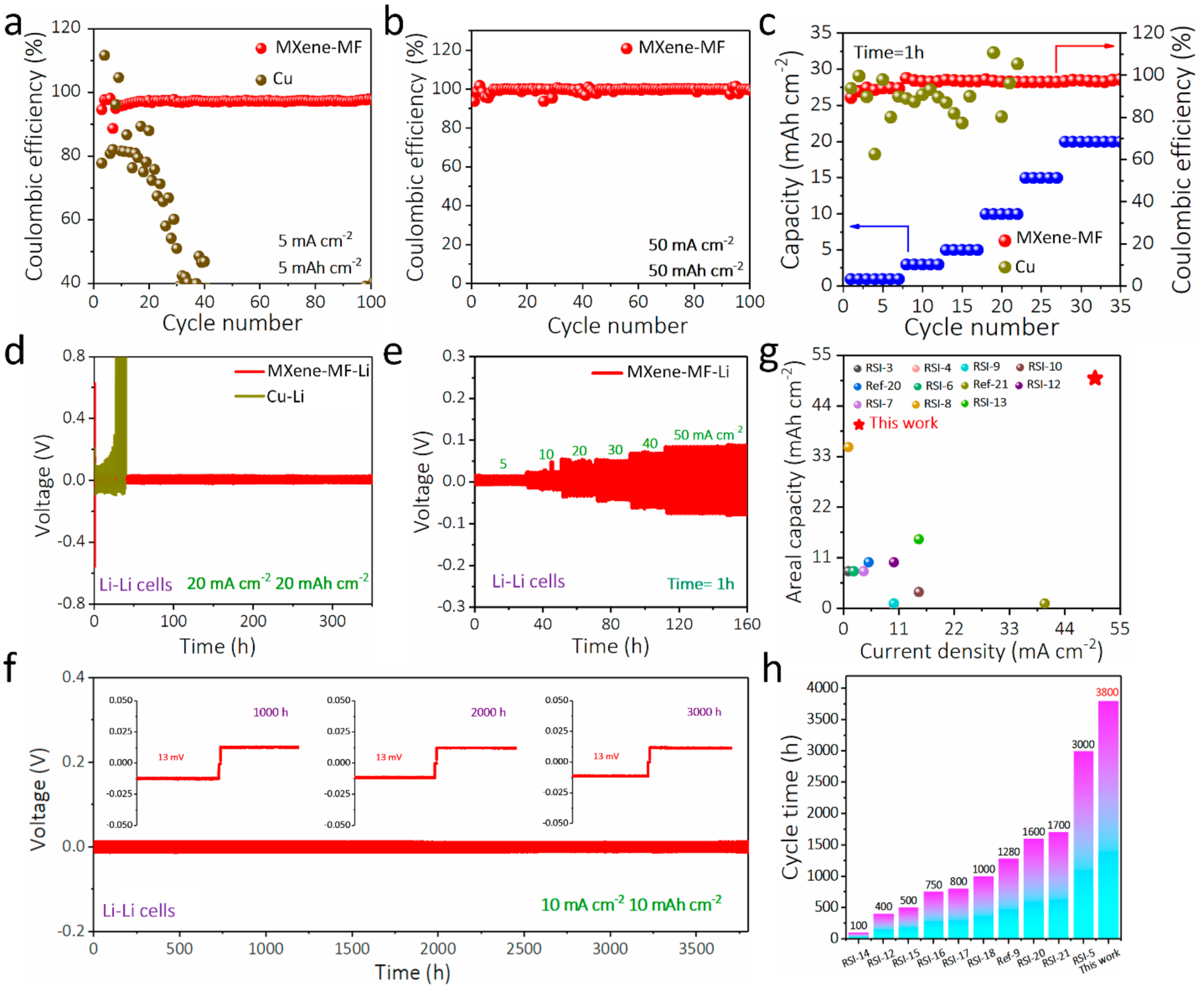

Figure 2. Electrochemical performance of 3D MXene-MF for a Li anode. (a) of 3D MXene-MF and bare Cu electrodes with a Li deposition capacity of 5 mAh cm^{-2} at 5 mA cm^{-2}. (b) CE of a 3D MXene-MF electrode at a high current density of 50 mA cm^{-2} for 50 mAh cm^{-2}. (c) of MXene-MF and Cu electrodes with increasing current densities from 1 to 20 mA cm^{-2} for 1 h at each cycle. (d) Galvanostatic cycling of symmetric cells based on MXene-MF-Li and Cu−Li electrodes at 20 mA cm^{-2} for 20 mAh cm^{-2}. (e) Rate capability of a symmetric cell based on an MXene-MF-Li anode measured at current densities of 5, 10, 20, 30, 40, and 50 mA cm^{-2} for 1 h. (f) Long-life symmetric cell galvanostatic cycling of an MXene-MF-Li electrode at 10 mA cm^{-2} with a Li deposition capacity of 10 mAh cm^{-2}. (g) Comparison of areal capacity *vs* current density of an MXene-MF-Li electrode with currently reported high-capacity Li composite anodes. (h) Cycle time comparison of an MXene-MF-Li electrode with the previously reported Li metal anodes stabilized by various strategies.

Figure 1b), which consists of predominantly single-layer, high-quality nanosheets, as evidenced by atomic force microscopy (AFM), scanning electron microscopy (SEM), and transmission electron microscopy (TEM). As shown in Figure 1c,d and Figure S2a, the MXene flakes possess a clean surface with few defects and are ~1.6 nm in thickness, indicative of high-quality, monolayer nanosheets, agreeing with previous reports.[40] The selected area electron diffraction (SAED, Figure S2b and inset of Figure 1d) the hexagonally packed atoms in the nanosheets, inherited from the MAX precursor. It is statistically revealed that the delaminated MXene nanosheets are distributed with an average lateral size of ~2.9 μm (Figure S2c).

After soaking, the sponge was freeze-dried to form flexible and lightweight 3D MXene-MF with a specific surface area of 24 m^2 g^{-1} (Figure S3). It can be observed that the color of the foam changes from white (pure MF) to black after immersing the MF in the MXene inks for 1 min (Figures S4, S5). The MXene-MF are highly conductive (25.5 Ω by multimeter, Figure S5) with a total mass density of 24.5−54.3 mg cm^{-2} (Table S1) easily tuned by adjusting the concentration of MXene ink or immersing time. It is noted that, unlike previously reported MXene-based 3D aerogels that are either fragile or rigid, the strong hydrogen bonding between MF (NH_2, NH, and imine) molecular chains and enriched surface functional groups (−OH, −F) of MXene guarantees the tight adhesion of MXene to the MF skeleton during the drying process, endowing excellent mechanical properties in the resultant 3D MXene-MF (Figure 1e).[41,42] The SEM image (Figure 1f) and energy-dispersive spectroscopy (EDS) elemental mapping (Figure 1g) indicate a thin layer of MXene nanosheets tightly attached on the surface of MF. X-ray diffraction (XRD) patterns and Fourier transform infrared (FTIR) spectroscopy (Figure 1h,i) reveal the coexistence of the characteristic peaks of MXene and MF in 3D MXene-MF. In particular, the blue shift of the absorption peaks of NH_2/

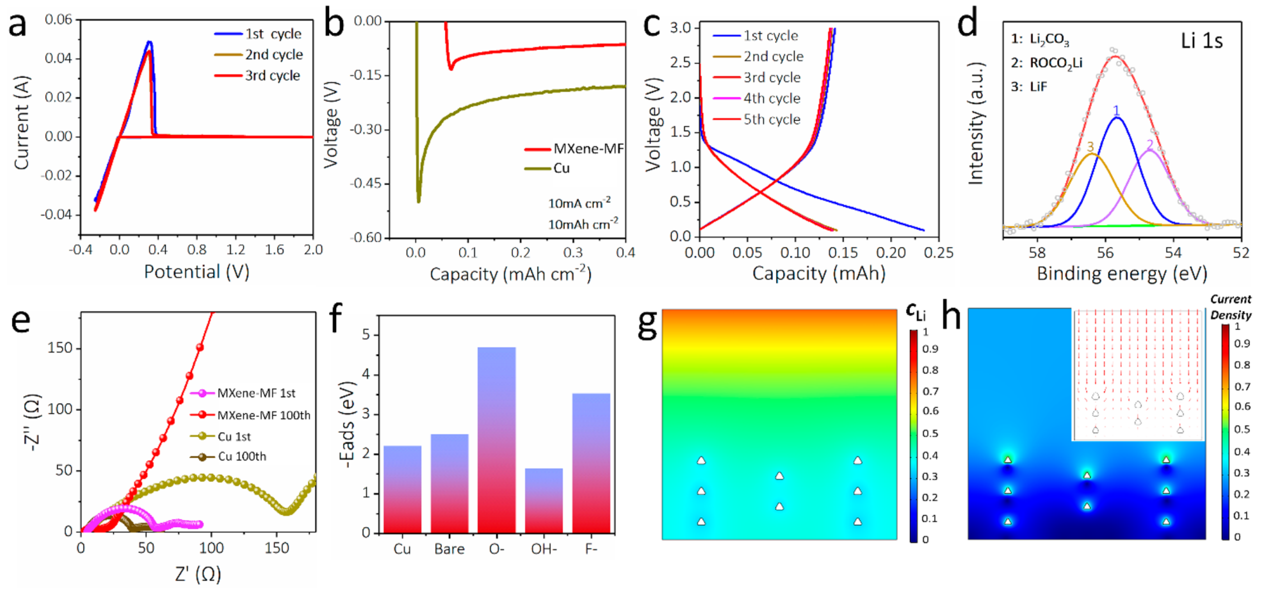

Figure 3. Mechanism illustration of 3D MXene-MF for a Li anode. (a) CVs of the MXene-MF electrode at a scan rate of 1 mV s^{-1}. (b) Nucleation section on the voltage profiles of MXene-MF and bare Cu electrodes at the first cycle. (c) Charge−discharge behavior of the MXene-MF electrode tested in the voltage range of 0.01−3 V at 200 μA at the first five cycles. (d) High-resolution Li 1s XPS spectrum of MXene-MF electrodes after 10 cycles. (e) Nyquist plots of MXene-MF-Li and bare Cu−Li electrodes before cycling and after the 100th cycle. (f) Binding energies of a Li atom with bare Cu, pure-MXene, O-MXene, OH-MXene, and F-MXene. (g, h) 2D transient model of (g) the Li ion concentration distribution (C_{Li}) and (h) current density distribution of the MXene-MF electrode in the electrolyte. Inset is the corresponding transport path of Li ions.

NH (3047 cm^{-1}) and imine (1592 cm^{-1}) to higher wavelengths of 3415 and 1602 cm^{-1}, respectively, is direct evidence of the formation of hydrogen bonding between MXene and MF molecular chains.[43] X-ray photoelectron spectroscopy (XPS, Figure 1j and Figure S6) indicates the presence of F from MXene in the MXene-MF, which plays a significant role in the alkali-metal plating and the formation of a solid electrolyte interphase (SEI), as will be discussed later.[28,44]

To examine the 3D MXene-MF in suppressing dendrite formation, the Coulombic efficiencies (CEs) of MXene-MF under various current densities are compared to those of the Cu electrode in an ether-based electrolyte. With a plating time of 1 h for each cycle, the CE of MXene-MF electrodes is 98% at 5 mA cm^{-2} for 100 cycles. Even the CE is low during the initial cycles due to the unstable SEI film, the CE quickly reached 99% at 10 mA cm^{-2} for 100 cycles, which is higher than those of the bare Cu electrode (40% for 40 cycles at 5 mA cm^{-2} and 30% for 10 cycles at 10 mA cm^{-2}) (Figure 2a and Figure S7). Impressively, MXene-MF can serve as a high Li utilization and stable scaffold for hosting ∼80% Li content and a high CE of 99% over 100 cycles and stably works (100 mV) at a high current density of 50 mA cm^{-2} for a high areal capacity of 50 mAh cm^{-2} (Figure 2b, Figure S8, and Table S2). Further, the rate performance is also evaluated at the same plating time (1 h). Unlike the bare Cu electrode, which decays rapidly as the current density increases over 3 mA cm^{-2}, the MXene-MF electrode maintains good stability along with a stepwise-increased current density from 1 to 20 mA cm^{-2} (Figure 2c).

To verify the superiority of the 3D scaffold electrode, the long-term voltage profile of symmetric cells based on MXene-MF-Li and pure Li was compared. It is revealed that the overpotential of the bare Li symmetric cell increases sharply to 0.8 V after 150 h, while the MXene-MF-Li cell shows a consistent and flat voltage profile with an overpotential of ∼13 mV after 700 h, at a current density of 5 mA cm^{-2} for 5 mAh cm^{-2} (Figure S9). Increasing the current density to 20 mA cm^{-2} with a cycling capacity of 20 mAh cm^{-2} slightly enlarges the voltage hysteresis (∼30 mV, Figure 2d). Also, the symmetric cell based on an MXene-MF-Li electrode is capable of charging−discharging up to 350 h without any signs of short circuit (Figure S10), implying good cycling stability. Besides, little voltage fluctuation is observed as the current density increases from 5 to 50 mA cm^{-2} at a settled stripping/plating time of 1 h (Figure 2e and Figure S11), demonstrating good rate performance. Impressively, our MXene-MF-Li electrode is capable of cycling for 3800 h, corresponding to 1900 cycles, at a high current density of 10 mA cm^{-2} (Figure 2f and Figure S12). It is worth noting that a high current density of 50 mA cm^{-2}, high capacity of 50 mAh cm^{-2}, and long cycling life (3800 h) in our MXene-MF-Li anode is better than most previously reported Li anodes (Figure 2g,h and Tables S3, S4), such as graphite microtubes (5 mA cm^{-2}, 10 mAh cm^{-2}, 3000 h),[45] carbon nanotubes (15 mA cm^{-2}, 15 mAh cm^{-2}, 600 h),[28] and 3D Ag/graphene (40 mA cm^{-2}, 1 mAh cm^{-2}, 5 h).[46]

In order to understand the mechanism of the MXene-MF for superior electrochemical performance, cyclic voltammograms (CVs) of the MXene-MF electrode were first tested at 1 mV s^{-1}, revealing almost unchanged Li plating (0.25 V, 38 mA) and stripping peaks (0.3 V, 43 mA) during cycling, indicative of extraordinarily uniform and stable Li nucleation and growth (Figure 3a). Unlike the bare Cu electrode with a striking overpotential of 0.5 V in the first cycle, the voltage curve of the MXene-MF electrode is flat at the nucleation stage with a small overpotential of 0.12 V, indicative of exceptional lithiophilicity of MXene-MF (Figure 3b).[47] Importantly, the CE reaches 99% after four cycles at 0.01−3 V, confirming the formation of the stable SEI layer on the MXene-MF electrodes (Figure 3c and Figure S13).[48] According to the XPS spectrum, the SEI layer

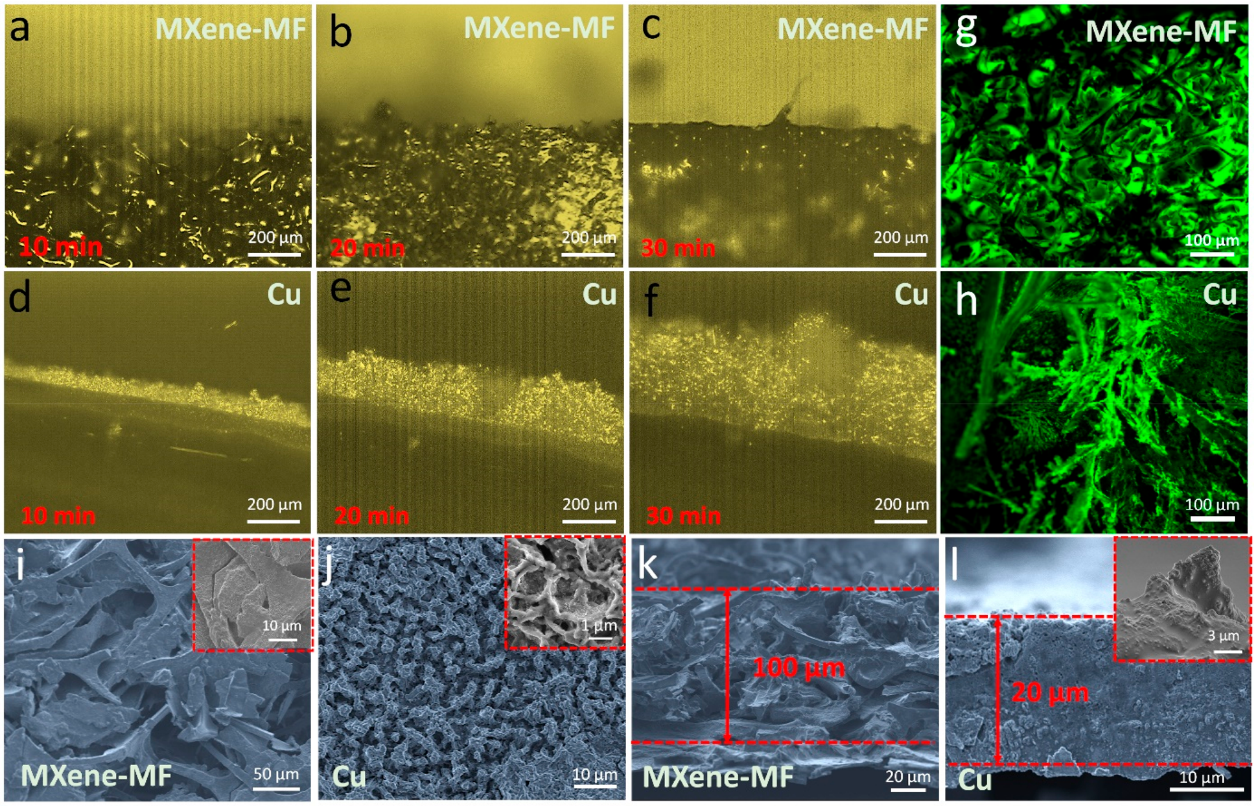

Figure 4. Morphologies of Li electrodeposition on 3D MXene-MF and bare Cu electrodes. (a−f) Cross-sectional *in situ* optical microscopy images of the Li electrodeposition process of (a−c) MXene-MF and (d−f) Cu electrodes at a current density of 2.0 mA cm^{-2} after 10, 20, and 30 min, respectively. (g, h) Fluorescence images of (g) MXene-MF and (h) Cu electrodes with a capacity of 2.0 mAh cm^{-2} at 2.0 mA cm^{-2}. (i, j) Top-view SEM images of (i) MXene-MF and (j) bare Cu electrodes with a Li plating capacity of 10 mAh cm^{-2} at 10 mA cm^{-2}. Insets are the corresponding magnified SEM images. (k, l) Cross-section SEM images of (k) MXene-MF and (l) bare Cu electrodes with a Li plating capacity of 10 mAh cm^{-2} at 10 mA cm^{-2}. Inset in (l) is the corresponding magnified SEM image.

consists of a majority of inorganic Li salts such as Li_2CO_3, $ROCO_2Li$, and LiF on cycled Li metal (Figure 3b and Figure S14).[38,49] Such a stable SEI layer enables a smaller charge transfer resistance (R_{ct}) of 40 Ω in the MXene-MF electrode compared to 160 Ω in the bare Cu electrode (Figure 3e), which could be reasonably attributed to the much enhanced Li ionic transport kinetics (1.58×10^{-8} cm^2 s^{-1}) in our MXene-MF (Figure S15).[50] Density functional theory (DFT) calculations imply that the surface O and F groups increase the binding energy of the Li atom to MXene substantially; 4.69 eV in O-terminated MXene and 3.53 eV in F-terminated MXene are much higher in comparison with the bare MXene (2.50 eV), Cu (2.21 eV), and OH-terminated MXene (1.64 eV) (Figure 3f and Figure S16). It is suggested that, by tuning the surface chemistry of MXene, such as increasing the content of F and/or O groups, the lithiophilicity of the 3D framework can be further optimized for uniform Li deposition, which is also suitable for Na and K atoms (Figure S17).

Finite element method (FEM) simulations were carried out to provide insightful understanding on spatial current density and Li ion concentration distributions. In contrast to the obvious Li ion starvation and a high current density on the bare Cu electrode (Figure S18), a higher Li ion concentration is realized in 3D MXene-MF (Figure 3g) coupled with a lower local current density (Figure 3h). As such, uniform and dendrite-free plating of lithium on the MXene-MF electrode surface is facilitated.[51]

To visualize the dendrite growth, the Li-plating process was observed by *in situ* optical microscopy (Figure S19). Figure 4a−f show the images taken at different states at the fixed current density of 2.0 mA cm^{-2}. A typical 3D porous structure is observed in the MXene-MF electrode and smooth and denser Li deposition without dendrite formation and volume expansion during Li plating (Figure 4a−c). In sharp contrast, inhomogeneous Li deposition with huge volume expansion (~400%) after 30 min of plating is found in the bare Cu electrode (Figure 4d−f). The fluorescence images corroborate the optical images, as a flat and uniform layer of Li on the 3D MXene-MF host is revealed (Figure 4g), in contrast to leaf-like Li dendrites generated on the Cu surface (Figure 4h and Figure S20). When increasing the current density by 2.5 (5 mAh cm^{-2}, Figure S21) and 5 times (10 mAh cm^{-2}, Figure 4i,k), the flat and smooth surface is well preserved in the 3D MXene-MF scaffold without Li dendrite. As for the bare Cu electrode, a large number of uneven pits emerge after cycling, indicative of the generation of dendritic Li and "dead Li" (Figure 4j,l and inset).

To demonstrate the generality of the 3D MXene-MF host in efficiently suppressing the dendrite formation and realizing high-performance metal anodes, we employed the host for plating Na (K) and assembled asymmetric Na (K)/Cu cells and Na (K)/MXene-MF cells, respectively. Notably, unlike the Cu electrode, which quickly decays at high current density, our Na/MXene-MF electrode maintains good stability with a high CE of 99% for 8 mA cm^{-2} (270 cycles) and 10 mA cm^{-2} (150

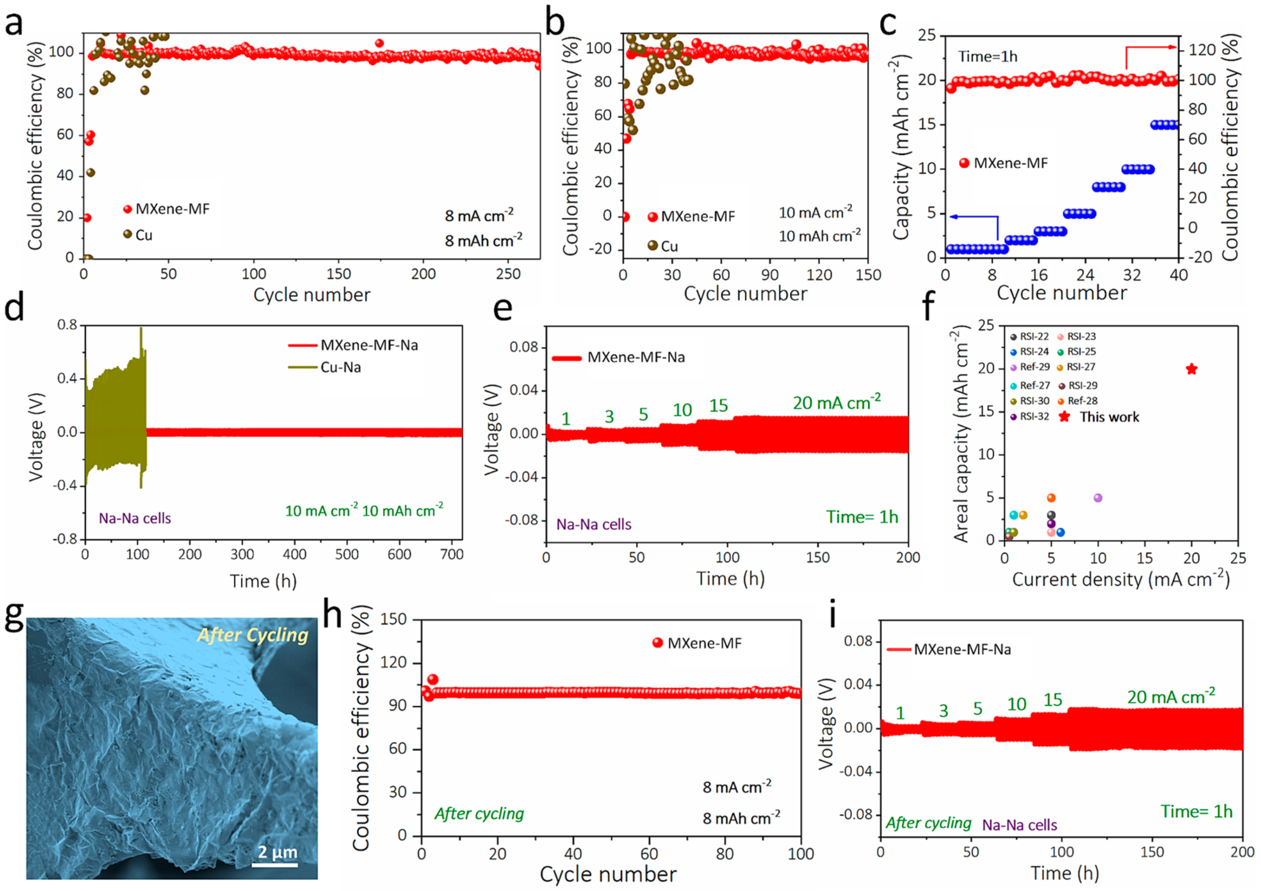

Figure 5. Electrochemical performance of 3D MXene-MF for the Na anode. (a, b) CEs of 3D MXene-MF and bare Cu electrodes with a Na deposition capacity of (a) 8 mAh cm^{-2} at 8 mA cm^{-2} and (b) 10 mAh cm^{-2} at 10 mA cm^{-2}. (c) CEs of MXene-MF and bare Cu electrodes with increasing current densities from 1 to 20 mA cm^{-2} for 1 h. (d) Galvanostatic cycling of symmetric cells based on MXene-MF-Na and Cu−Na electrodes at 10 mA cm^{-2} for 10 mAh cm^{-2}. (e) Rate capability of symmetric cells based on MXene-MF-Na electrodes. (f) Comparison of areal capacity *vs* current density of an MXene-MF-Na electrode with currently reported high areal capacity Na composite anodes. (g) SEM image of MXene-MF with sodium stripping after cycling. (h) CE of an MXene-MF electrode with a Na deposition capacity of 8 mAh cm^{-2} at 8 mA cm^{-2} for 100 cycles. (i) Rate performance of a symmetric cell of an MXene-MF-Na electrode with increasing current densities from 1 to 20 mA cm^{-2} for 1 h.

cycles) (Figure 5a,b). Furthermore, Na/MXene-MF cells provide a high CE of 99% obtained even under a high current density of 15 mA cm^{-2} (40 cycles), indicative of high rate capability achieved (Figure 5c). Besides, the MXene-MF-Na symmetric cells show consistent and flat voltage profiles for 720 h at 10 mA cm^{-2}, originating from a stable electrode interface (73 and 63 Ω at the initial state and after the 100th cycle, respectively, Figure 5d and Figure S22). Upon raising the current density up to 20 mA cm^{-2} for 1h, the MXene-MF-Na cells display a small hysteresis of ∼15 mV without short circuit (Figure 5e and Figure S23). We note that the high rate (20 mA cm^{-2}, 20 mAh cm^{-2}) of the MXene-MF-Na cells has greatly surpassed the rate of reported sodium anodes (Figure 5f and Table S5), such as porous Cu (1 mA cm^{-2}, 1 mAh cm^{-2}),[52] rGO (5 mA cm^{-2}, 5 mAh cm^{-2}),[53] and Ti_3C_2−Sn (10 mA cm^{-2}, 5 mAh cm^{-2}).[54] Further, unlike the bare Cu electrode with a CE below 50% after 10 cycles, the MXene-MF electrode showcases a high and stable CE of 96% for 55 cycles, coupled with a long cycling stability of 800 h at 5 mAh cm^{-2} at 5 mA cm^{-2} (Figure S24a,b). In addition, the MXene-MF-K symmetric cell shows smaller charge transfer resistance of 311 Ω at the first cycle and 117 Ω after the 100th cycle, in comparison with a pure K cell (74 Ω at the first cycle and 30 Ω after the 100th cycle, Figure S25), demonstrative of a good rate capability and stable voltage amplification when the current density stepwise increases from 1 to 7 mA cm^{-2} (Figure S26).

Actually, our 3D conductive flexible MXene-MF host exhibits a high mechanical integrity and good recyclability. As seen in Figure 5g, the lithiophilic MXene nanosheets are still attached firmly on the surface of the 3D MF framework without any signs of delamination after washing the cycled electrode with ethyl alcohol and dilute hydrochloric acid (Figure S27). Importantly, when plating Li or Na on this reused MXene-MF electrode, a high CE (99%, 100 cycles) and long-term cycling stability (Figure 5h,i and Figure S28) are achieved, indicative of outstanding recoverability of our 3D MXene-MF. We note the excellent recyclability of metal anodes could be attributed to the lithiophilic surface of MXene. For comparison, when coating other conductive inks with poor lithiophilicity and conductivity such as electrochemically exfoliated graphene (EG, 10 mg mL^{-1}, Figure S29)[55] or PH1000 conducting polymers, the resulting 3D MF-based electrodes exhibit apparently decreased cycling stability than that of MXene-MF (Figures S30, S31).

We further demonstrate the application of our high-performance anode in pouch cells by pairing an MXene-MF-

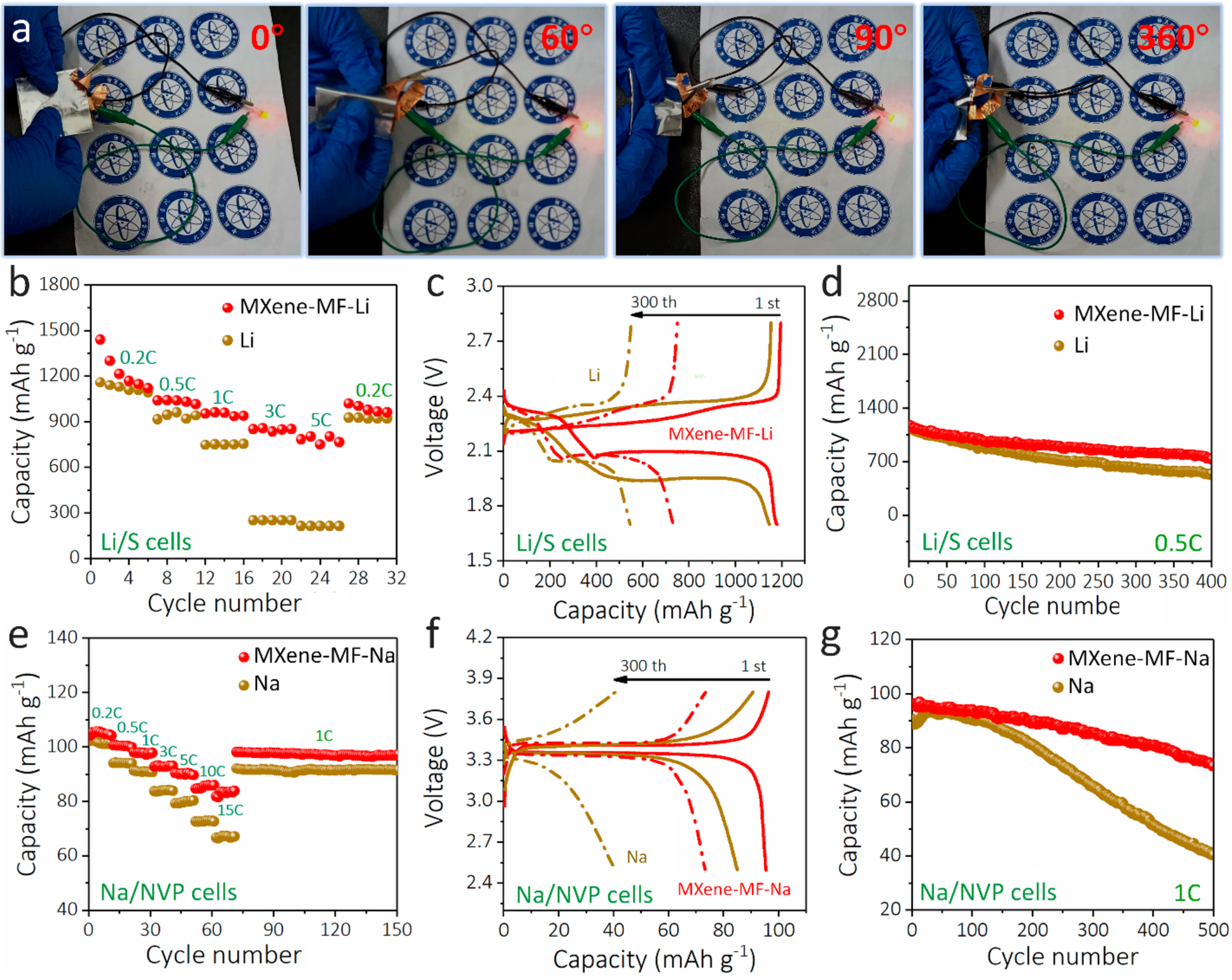

Figure 6. Electrochemical performance of an MXene-MF-based alkali-metal full battery. (a) Photographs of an LED lit by soft-packaged MXene-MF-Li/MXene-MF-S batteries taken at different folding angles. The use of the logo is permitted from Dalian Institute of Chemical Physics, Chinese Academy of Sciences. (b) Rate capability, (c) charge and discharge profiles, and (d) cycling stability for 300 cycles tested at 0.5 C (1.0 C = 1675 mAh g^{-1} for the S cathode) of MXene-MF-Li/S and pure Li/S batteries. (e) Rate capability, (f) charge and discharge profiles, and (g) cycling stability for 500 cycles tested at 1 C (1.0 C = 117.6 mAh g^{-1} for NVP cathode) of MXene-MF-Na/NVP and pure Na/NVP batteries.

Li anode with a high mass loading sulfur (S) MXene-MF cathode (5 mg cm^{-2}, without conductive agent and binder, Figure S32). As shown in Figure 6a, a light emitting diode (LED) is readily powered by an MXene-MF-Li/S pouch cell under different bending degrees (0°, 60°, 90°, and 360°) without an obvious change in brightness, indicative of great potential of our flexible anodes in wearable electronics. Further, the MXene-MF-Li/S button cell consistently exhibits an improved rate capability as well as long-term cycling performance compared with that of a pure Li/S cell (based on the mass of S, Figure 6b and Figure S33). For instance, the MXene-MF-Li/S cell delivers 858 mAh g^{-1} at 3 C, 804 mAh g^{-1} at 5 C, and a capacity retention of 62% after cycling 400 times with nearly 100% CE (Figure S34), against (253 mAh g^{-1}, 214 mAh g^{-1}, 47%) in a pure Li/S cell (Figure 6c,d). The polarization potential of the MXene-MF-Li/S cell is only 167 mV, in sharp contrast to that of a pure Li/S cell (408 mV, Figure S35).

Impressively, the MXene-MF-Na/NVP cell exhibits a good performance (based on the mass of NVP), *e.g.*, 86 and 84 mAh g^{-1} at high rates of 10 and 15 C, respectively (Figure 6e and Figure S36). The specific capacity is considerably higher than that of a pure Na/NVP cell (72 mAh g^{-1} at 10 C, 67 mAh g^{-1} at 15 C). Such a difference becomes even more apparent when cycling the two cells for 500 times at 1 C, as the MXene-MF-Na/NVP cell maintains a capacity of 74 mAh g^{-1} with a CE of nearly 100% (Figure S37), being 55% higher than the counterpart (41 mAh g^{-1}).

We believe several key factors are responsible for the excellent performance of these dendrite-free alkali-metal anodes. First, the inherent high electrical conductivity in MXene accelerates the electron transport while significantly reducing the akali-metal ion concentration polarization (Figure 3g). Second, the 3D interconnected macroporous scaffold with well-distributed conductive and lithiophilic MXene nanosheets efficiently ensures an uniform ion flux and reduces the local current density for homogeneous high-capacity alkali-metal deposition (Figure 3h). Third, the excellent mechanical toughness of MF and outstanding electrochemical stability of MXene nanosheets significantly buffer the huge volume change and internal stress fluctuations, maintaining the electrode structural integrity during fast and deep alkali-metal plating and stripping. As a result, dendrite-free alkali-metal deposition within the entire 3D framework has been realized at both high current densities and high deposition capacities.

CONCLUSIONS

In summary, we develop a lightweight 3D MXene-MF conductive scaffold for stable and high-performance alkali-metal anodes. Owing to their favorable lithiophilic surface, fast electronic and ionic transport channels, and superior mechanical strength, the 3D MXene-MF host suppresses the dendritic growth and infinite volume change of alkali-metal anodes. Consequently, a high current density of 50 mA cm^{-2} and 50 mAh cm^{-2} for the Li anode and a high rate of 20 mA cm^{-2} for 20 mAh cm^{-2} for the Na anode have been simultaneously achieved, coupled with a long cycle life. We further demonstrate MXene-MF-alkali meal anode-based full batteries, showcasing substantially improved rate capability and cycling stability. This rational structural design of an alkali-metal anode sheds light on the development of the advanced high-energy-density and high-safety alkali-metal batteries.

METHODS

Preparation of 3D MXene-MF. $Ti_3C_2T_X$ MXene was prepared from Ti_3AlC_2 by LiF/HCl etchants previously reported.[56] EG was prepared by an electrochemical exfoliation method by a two-electrode system.[55] After that, the commercial MF was first cut into a desirable thickness and shape and then soaked in the homogeneous MXene ink (10 mg mL^{-1}) for 1 min to form wet MF filled with MXene nanosheets. After freeze-drying for 3 days, 3D MXene-MF (25 mg cm^{-2}) was obtained. For high mass density MXene-MF electrodes with 40 and 50 mg cm^{-2}, the concentrations of MXene ink used were 15 and 20 mg mL^{-1}, respectively. The EG-MF and PH1000-MF were also prepared by replacing MXene ink with EG (10 mg mL^{-1}) and PH1000 solution while the other steps remained unchanged.

Preparation of NVP. NVP was synthesized in terms of previously reported work.[57] Typically, 0.7 g of vanadium pentoxide and 1.5 g of oxalic acid were dispersed into deionized water at 70 °C and stirred for 1 h. Then, 1.8 g of sodium dihydrogen phosphate and 0.4 g of glucose were added into the above dispersion with stirring for 1 h, followed by the addition of 100 mL of *n*-propanol. After the obtained solution was dried in an oven overnight, the mixture was heated at 800 °C for 4 h in a 5% N_2/H_2 atmosphere (95%/5% in volume ratio) and NVP was obtained.

Material Characterization. The morphology and structure of materials and electrodes were characterized by SEM (JEOL JSM-7800F), TEM (JEM-2100), AFM (Veeco nanoscope multimode II-D), XPS (Thermo ESCALAB 250Xi equipped with a monochromatic Al Kα source of 1486.5 eV), FTIR (Bruker, Hyperion 3000), XRD (Empyrean with Cu Kα radiation in the 2θ range from 5° to 90°), Mastersizer 2000 (Malvern Instruments, UK), Olympus FV1000 MPE confocal laser scanning microscope (Olympus), and nitrogen adsorption and desorption isotherm (Quadrasorb SI).

Electrochemical Measurement. All the cells were assembled with standard CR2025 coin-type cells in an Ar-filled glovebox with O_2 and H_2O content below 0.5 ppm. In the Li metal-based tests, the electrolyte employed was 1.0 M lithium bis(trifluoromethanesulfonyl) imide (LiTFSI) in a mixture solution of 1,3-dioxolane (DOL) and 1,2-dimethoxyethane (DME) (1:1, vol. ratio) with 1 wt % $LiNO_3$ as additive. For the Na metal based measurement, the electrolyte employed was 1.0 M sodium hexafluorophosphate ($NaPF_6$) in bis(2-methoxyethyl) (DIGLYME). As for the K metal-based test, 0.8 M potassium bis(fluoroslufonyl)imide (KFSI) in a mixture solution of ethylene carbonate (EC) and diethyl carbonate (DEC) was used. For Li metal, about 40 μL of electrolyte was dropped into each cell, and the polypropylene membrane (Celgard 2500) was used as the separator,. For Na and K metal, a glass microfiber filter (Whatman) was used as the separator, and about 100 μL of electrolyte was used in each cell. MXene-MF and bare Cu were used as the working electrodes, and alkali-metal foil was used as the counter/reference electrodes to evaluate the CE. The assembled cells were precycled between 0.01 and 3 V at 100 μA for five times to stabilize the SEI film formation and remove surface contaminations. Afterward, a certain capacity of alkali metal was deposited onto the current collector and then charged to 1 V to strip the alkali metal at a certain current density for each cycle on a LAND CT2001A battery system. For the symmetric cells, about 20% excess capacity alkali metal anode was first predeposited onto the current collector. Then, the cells were disassembled and the symmetric cell configurations were assembled with an MXene-MF-alkali metal or pure alkali metal anode to evaluate the long-time cycling stability. S powder (99.9%) was purchased from Sigma-Aldrich. For the full cells, the working electrode contains 80 wt % active materials (S or NVP), 10 wt % carbon black, and 10 wt % polyvinylidene fluoride with *N*-methyl-2-pyrrolidone as the solvent. For the pouch cells, the S slurry was directly coated on the MXene-MF scaffold with a high S loading of 5 mg cm^{-2}. For the button cells, the (S or NVP) slurry was cast onto carbon-coated Al foil using the doctor. The cast electrodes were dried under vacuum at 55 °C (S) and 120 °C (NVP) for 12 h. The sulfur cathode with a sulfur loading of ~1.0 mg cm^{-2} was employed in Li−S cells, using 1.0 M LiTFSI in DOL/DME (v/v = 1:1) with 1.0 wt % $LiNO_3$ as electrolyte in the Li−S cells, and about 40 μL of electrolyte was added into each cell. The cathode with an NVP loading of ~2.0 mg cm^{-2} was employed in the MXene-MF-Na/NVP full cells, using 1.0 M sodium perchlorate ($NaClO_4$) in propylene carbonate (PC) with 5 wt % fluoroethylene carbonate (FEC) as additive as the electrolyte. The CV curves at a scan rate of 0.1 mV s^{-1} and the EIS by applying an ac amplitude of 5 mV over the frequency range of 100 kHz to 0.01 Hz were carried out on a CHI 760E electrochemical workstation. The *in situ* optical microscopy experiment was performed on the transparent quartz cell. Typically, the MXene-MF and Cu foil electrodes together with bare Li foil were assembled in a sealed quartz cell containing 1.0 M LiTFSI in EC/DMC (1:1, vol. ratio) electrolyte inside a glovebox to visually compare the dendrite growth behavior by optical microscopy (VK-8510, KEYENCE).

Computational Simulation. A 2D transient model was constructed by coupling the Nernst−Planck equation with the Butler−Volmer equation to model the lithium ion deposition process. The initial concentration of Li ion was set to be 1 M, and the operation current density was 20 mA cm^{-2}. The model was built by employing the tertiary current distribution and Nernst−Planck interface and solved by COMSOL Multiphysics using the finite element method. The relative error tolerance was 1×10^{-6}. DFT calculations have been performed with the DMol3 package.[58] In the framework of DFT, the generalized gradient approximation (GGA) combined with the Perdew−Burke−Enzerhof (PBE) functional was employed to describe the exchange and correlation potential.[59,60] All the atoms of the calculated systems are allowed to fully relax in order to optimize the adsorption geometries. A double-numerical basis with polarization functions (DNP) is utilized to expand the valence electron functions into a set of numerical atomic orbitals, and the DFT semicore pseudopotential (DSPP) is used when tackling the electron−ion interactions. The *k*-point mesh in the Monkhorst Pack sampling scheme was set as 1 × 1 × 1.[61] The Fermi smearing is set to 5.0×10^{-3} Ha (1 Ha = 27.21 eV). For the convergence criteria, the SCF tolerance used was 1.0×10^{-5} eV atom^{-1}, and the maximum force and displacement were set as 5.0×10^{-2} eV Å^{-1} and 2.0×10^{-3} Å, respectively. For the alkali-metal atom combined with Cu and MXene,[62,63] the binding energy (E_b) is defined as the energy difference between the substrate with an alkali atom (E_t) and the summation of the alkali-metal atom (E_1) and substrate system (E_2): $E_a = E_1 + E_2 - E_t$.

ASSOCIATED CONTENT

Supporting Information

The Supporting Information is available free of charge at https://pubs.acs.org/doi/10.1021/acsnano.0c03042.

Materials characterization, electrochemical characterization, details of computational simulation, additional figures, and the table used for characterization of MF-MXene and performance comparison of our MF-MXene-based alkali metal (Li, Na) anodes with the state-of-the-art alkali metal (Li, Na) anodes; Figures S1−S37; Tables S1−S5 (PDF)

AUTHOR INFORMATION

Corresponding Authors

Qiong Zheng − *Division of Energy Storage, Dalian National Laboratory for Clean Energy, Dalian Institute of Chemical Physics, Chinese Academy of Sciences, Dalian 116023, China;* orcid.org/0000-0002-1659-0549; Email: zhengqiong@dicp.ac.cn

Yan Yu − *Hefei National Laboratory for Physical Sciences at the Microscale, Department of Materials Science and Engineering, Key Laboratory of Materials for Energy Conversion, University of Science and Technology of China, Hefei, Anhui 230026, China;* orcid.org/0000-0002-3685-7773; Email: yanyumse@ustc.edu.cn

Zhong-Shuai Wu − *2D Materials & Energy Devices Lab, Dalian National Laboratory for Clean Energy, Dalian Institute of Chemical Physics, Chinese Academy of Sciences, Dalian 116023, China;* orcid.org/0000-0003-1851-4803; Email: wuzs@dicp.ac.cn

Authors

Haodong Shi − *2D Materials & Energy Devices Lab, Dalian National Laboratory for Clean Energy, Dalian Institute of Chemical Physics, Chinese Academy of Sciences, Dalian 116023, China; University of Chinese Academy of Sciences, Beijing 100049, China*

Meng Yue − *University of Chinese Academy of Sciences, Beijing 100049, China; Division of Energy Storage, Dalian National Laboratory for Clean Energy, Dalian Institute of Chemical Physics, Chinese Academy of Sciences, Dalian 116023, China*

Chuanfang John Zhang − *Swiss Federal Laboratories for Materials Science and Technology (Empa), CH-8600 Dübendorf, Switzerland*

Yanfeng Dong − *Department of Chemistry, College of Sciences, Northeastern University, Shenyang 110819, China*

Pengfei Lu − *2D Materials & Energy Devices Lab, Dalian National Laboratory for Clean Energy, Dalian Institute of Chemical Physics, Chinese Academy of Sciences, Dalian 116023, China*

Shuanghao Zheng − *2D Materials & Energy Devices Lab, Dalian National Laboratory for Clean Energy, Dalian Institute of Chemical Physics, Chinese Academy of Sciences, Dalian 116023, China*

Huijuan Huang − *Hefei National Laboratory for Physical Sciences at the Microscale, Department of Materials Science and Engineering, Key Laboratory of Materials for Energy Conversion, University of Science and Technology of China, Hefei, Anhui 230026, China*

Jie Chen − *University of Chinese Academy of Sciences, Beijing 100049, China; Key Laboratory of Separation Science for Analytical Chemistry, Dalian Institute of Chemical Physics, Chinese Academy of Sciences, Dalian 116023, China*

Pengchao Wen − *2D Materials & Energy Devices Lab, Dalian National Laboratory for Clean Energy, Dalian Institute of Chemical Physics, Chinese Academy of Sciences, Dalian 116023, China*

Zhaochao Xu − *Key Laboratory of Separation Science for Analytical Chemistry, Dalian Institute of Chemical Physics, Chinese Academy of Sciences, Dalian 116023, China;* orcid.org/0000-0002-2491-8938

Xianfeng Li − *Division of Energy Storage, Dalian National Laboratory for Clean Energy, Dalian Institute of Chemical Physics, Chinese Academy of Sciences, Dalian 116023, China;* orcid.org/0000-0002-8541-5779

Complete contact information is available at: https://pubs.acs.org/10.1021/acsnano.0c03042

Author Contributions

Z.-S. Wu proposed and supervised the overall project. H. D. Shi prepared the samples and performed the electrochemical measurements. C. F. Zhang, Y. F. Dong, and S. H. Zheng prepared the MXene ink. H. D. Shi, M. Yue, C. F. Zhang, Q. Zheng, Y. Yu, and Z.-S. Wu analyzed the data. M. Yue and Q. Zheng did the FEM simulations. P. F. Lu did the DFT calculations. H. J. Huang and Y. Yan prepared the NVP materials. P. C. Wen performed the SEM and TEM measurements. J. Chen and Z. C. Xu performed fluorescence analysis. H. D. Shi, M. Yue, C. F. Zhang, Z. C. Xu, X. F. Li, Q. Zheng, Y. Yu, and Z.-S. Wu wrote the paper. All the authors discussed the results and commented on the manuscript. All the authors have given approval to the final version of the manuscript.

Author Contributions

[‖]H. D. Shi, M. Yue, and C. F. Zhang contributed equally to this work.

Notes

The authors declare no competing financial interest.

ACKNOWLEDGMENTS

This work was financially supported by the National Key R&D Program of China (Grant 2016YFA0200200), National Natural Science Foundation of China (Grants 51872283, 21805273, 51925207, 51872277, and U1910210), Liaoning BaiQianWan Talents Program, LiaoNing Revitalization Talents Program (Grant XLYC1807153), Natural Science Foundation of Liaoning Province, Joint Research Fund Liaoning-Shenyang National Laboratory for Materials Science (Grant 20180510038), DICP (DICP ZZBS201708, DICP ZZBS201802), DICP&QIBEBT (Grant DICP&QIBEBT UN201702), Dalian National Laboratory for Clean Energy (DNL), CAS, DNL Cooperation Fund, CAS (DNL180310, DNL180308, DNL201912, and DNL201915), and the Fundamental Research Funds for the Central Universities (WK2060140026).

REFERENCES

(1) Kang, K.; Meng, Y. S.; Bréger, J.; Grey, C. P.; Ceder, G. Electrodes with High Power and High Capacity for Rechargeable Lithium Batteries. *Science* **2006**, *311*, 977−980.

(2) Choi, J. W.; Aurbach, D. Promise and Reality of Post-Lithium-Ion Batteries with High Energy Densities. *Nat. Rev. Mater.* **2016**, *1*, 16013.

(3) Armand, M.; Tarascon, J.-M. Building Better Batteries. *Nature* **2008**, *451*, 652−657.

(4) Schmuch, R.; Wagner, R.; Hörpel, G.; Placke, T.; Winter, M. Performance and Cost of Materials for Lithium-Based Rechargeable Automotive Batteries. *Nat. Energy* **2018**, *3*, 267−278.

(5) Zhao, C.; Lu, Y.; Yue, J.; Pan, D.; Qi, Y.; Hu, Y.-S.; Chen, L. Advanced Na Metal Anodes. *J. Energy Chem.* **2018**, *27*, 1584−1596.

(6) Xiao, N.; McCulloch, W. D.; Wu, Y. Reversible Dendrite-Free Potassium Plating and Stripping Electrochemistry for Potassium Secondary Batteries. *J. Am. Chem. Soc.* **2017**, *139*, 9475−9478.

(7) Wang, Y. X.; Wang, Y. X.; Wang, Y. X.; Feng, X. M.; Chen, W. H.; Ai, X. P.; Yang, H. X.; Cao, Y. L. Developments and Perspectives on Emerging High-Energy-Density Sodium-Metal Batteries. *Chem.* **2019**, *5*, 2547−2570.

(8) Peng, H.-J.; Huang, J.-Q.; Zhang, Q. A Review of Flexible Lithium-Sulfur and Analogous Alkali Metal-Chalcogen Rechargeable Batteries. *Chem. Soc. Rev.* **2017**, *46*, 5237−5288.

(9) Bruce, P. G.; Freunberger, S. A.; Hardwick, L. J.; Tarascon, J. M. Li-O_2 and Li-S Batteries with High Energy Storage. *Nat. Mater.* **2012**, *11*, 19−29.

(10) Peng, Z. Q.; Freunberger, S. A.; Chen, Y. H.; Bruce, P. G. A Reversible and Higher-Rate Li-O_2 Battery. *Science* **2012**, *337*, 563−566.

(11) Takechi, K.; Shiga, T.; Asaoka, T. A Li-O_2/CO_2 Battery. *Chem. Commun.* **2011**, *47*, 3463−3465.

(12) Wang, Y. X.; Zhang, B. W.; Lai, W. H.; Xu, Y. F.; Chou, S. L.; Liu, H. K.; Dou, S. X. Room-Temperature Sodium-Sulfur Batteries: A Comprehensive Review on Research Progress and Cell Chemistry. *Adv. Energy Mater.* **2017**, *7*, 1602829.

(13) Xin, S.; Chang, Z.; Zhang, X.; Guo, Y.-G. Progress of Rechargeable Lithium Metal Batteries Based on Conversion Reactions. *Natl. Sci. Rev.* **2017**, *4*, 54−70.

(14) Goodenough, J. B.; Kim, Y. Challenges for Rechargeable Li Batteries. *Chem. Mater.* **2010**, *22*, 587−603.

(15) Palomares, V.; Serras, P.; Villaluenga, I.; Hueso, K. B.; Carretero-Gonzalez, J.; Rojo, T. Na-Ion Batteries, Recent Advances and Present Challenges to Become Low Cost Energy Storage Systems. *Energy Environ. Sci.* **2012**, *5*, 5884−5901.

(16) Zhao, Y.; Adair, K. R.; Sun, X. L. Recent Developments and Insights into the Understanding of Na Metal Anodes for Na-Metal Batteries. *Energy Environ. Sci.* **2018**, *11*, 2673−2695.

(17) Tikekar, M. D.; Choudhury, S.; Tu, Z. Y.; Archer, L. A. Design Principles for Electrolytes and Interfaces for Stable Lithium-Metal Batteries. *Nat. Energy* **2016**, *1*, 1−7.

(18) Li, W. Y.; Yao, H. B.; Yan, K.; Zheng, G. Y.; Liang, Z.; Chiang, Y. M.; Cui, Y. The Synergetic Effect of Lithium Polysulfide and Lithium Nitrate to Prevent Lithium Dendrite Growth. *Nat. Commun.* **2015**, *6*, 7436.

(19) Ding, F.; Xu, W.; Graff, G. L.; Zhang, J.; Sushko, M. L.; Chen, X.; Shao, Y.; Engelhard, M. H.; Nie, Z.; Xiao, J. Dendrite-Free Lithium Deposition *via* Self-Healing Electrostatic Shield Mechanism. *J. Am. Chem. Soc.* **2013**, *135*, 4450−4456.

(20) Wang, H.; Wang, C.; Matios, E.; Li, W. Facile Stabilization of the Sodium Metal Anode with Additives: Unexpected Key Role of Sodium Polysulfide and Adverse Effect of Sodium Nitrate. *Angew. Chem., Int. Ed.* **2018**, *57*, 7734−7737.

(21) Jiang, Z.; Wang, S.; Chen, X.; Yang, W.; Yao, X.; Hu, X.; Han, Q.; Wang, H. Tape-Casting $Li_{0.34}La_{0.56}TiO_3$ Ceramic Electrolyte Films Permit High Energy Density of Lithium-Metal Batteries. *Adv. Mater.* **2020**, *32*, 1906221.

(22) Han, X.; Gong, Y.; Fu, K.; He, X.; Hitz, G. T.; Dai, J.; Pearse, A.; Liu, B.; Wang, H.; Rublo, G.; Mo, Y.; Thangadurai, V.; Wachsman, E. D.; Hu, L. Negating Interfacial Impedance in Garnet-Based Solid-State Li Metal Batteries. *Nat. Mater.* **2017**, *16*, 572−579.

(23) Yan, K.; Lu, Z. D.; Lee, H. W.; Xiong, F.; Hsu, P. C.; Li, Y. Z.; Zhao, J.; Chu, S.; Cui, Y. Selective Deposition and Stable Encapsulation of Lithium through Heterogeneous Seeded Growth. *Nat. Energy* **2016**, *1*, 16010.

(24) Liu, Y. Y.; Lin, D. C.; Liang, Z.; Zhao, J.; Yan, K.; Cui, Y. Lithium-Coated Polymeric Matrix as a Minimum Volume-Change and Dendrite-Free Lithium Metal Anode. *Nat. Commun.* **2016**, *7*, 10992.

(25) Wang, C.; Xie, H.; Zhang, L.; Gong, Y.; Pastel, G.; Dai, J.; Liu, B.; Wachsman, E. D.; Hu, L. Universal Soldering of Lithium and Sodium Alloys on Various Substrates for Batteries. *Adv. Energy Mater.* **2018**, *8*, 1701963.

(26) Zhang, R.; Li, N. W.; Cheng, X. B.; Yin, Y. X.; Zhang, Q.; Guo, Y. G. Advanced Micro/Nanostructures for Lithium Metal Anodes. *Adv. Sci.* **2017**, *4*, 1600445.

(27) Cheng, X. B.; Zhang, R.; Zhao, C. Z.; Zhang, Q. Toward Safe Lithium Metal Anode in Rechargeable Batteries: A Review. *Chem. Rev.* **2017**, *117*, 10403−10473.

(28) Li, Q.; Zhu, S.; Lu, Y. 3D Porous Cu Current Collector/Li-Metal Composite Anode for Stable Lithium-Metal Batteries. *Adv. Funct. Mater.* **2017**, *27*, 1606422.

(29) Chi, S.-S.; Liu, Y.; Song, W.-L.; Fan, L.-Z.; Zhang, Q. Prestoring Lithium into Stable 3D Nickel Foam Host as Dendrite-Free Lithium Metal Anode. *Adv. Funct. Mater.* **2017**, *27*, 1700348.

(30) Xie, J.; Ye, J.; Pan, F.; Sun, X.; Ni, K.; Yuan, H.; Wang, X.; Shu, N.; Chen, C.; Zhu, Y. Incorporating Flexibility into Stiffness: Self-Grown Carbon Nanotubes in Melamine Sponges Enable a Lithium-Metal-Anode Capacity of 15 mA h cm^{-2} Cyclable at 15 mA cm^{-2}. *Adv. Mater.* **2018**, *31*, 1805654.

(31) Shi, H.; Zhang, C. J.; Lu, P.; Dong, Y.; Wen, P.; Wu, Z.-S. Conducting and Lithiophilic MXene/Graphene Frameworks for High-Capacity, Dendrite-Free Lithium-Metal Anodes. *ACS Nano* **2019**, *13*, 14308.

(32) Deng, W.; Zhou, X.; Fang, Q.; Liu, Z. Microscale Lithium Metal Stored inside Cellular Graphene Scaffold toward Advanced Metallic Lithium Anodes. *Adv. Energy Mater.* **2018**, *8*, 1703152.

(33) Anasori, B.; Lukatskaya, M. R.; Gogotsi, Y. 2D Metal Carbides and Nitrides (MXenes) for Energy Storage. *Nat. Rev. Mater.* **2017**, *2*, 16098.

(34) Zhang, C. J.; McKeon, L.; Kremer, M. P.; Park, S. H.; Ronan, O.; Seral-Ascaso, A.; Barwich, S.; Coileain, C. O.; McEvoy, N.; Nerl, H. C.; Anasori, B.; Coleman, J. N.; Gogotsi, Y.; Nicolosi, V. Additive-Free MXene Inks and Direct Printing of Micro-Supercapacitors. *Nat. Commun.* **2019**, *10*, 1795.

(35) Pang, J.; Mendes, R. G.; Bachmatiuk, A.; Zhao, L.; Ta, H. Q.; Gemming, T.; Liu, H.; Liu, Z.; Rummeli, M. H. Applications of 2D MXenes in Energy Conversion and Storage Systems. *Chem. Soc. Rev.* **2019**, *48*, 72−133.

(36) Li, B.; Zhang, D.; Liu, Y.; Yu, Y.; Li, S.; Yang, S. Flexible Ti_3C_2 MXene-Lithium Film with Lamellar Structure for Ultrastable Metallic Lithium Anodes. *Nano Energy* **2017**, *39*, 654−661.

(37) Tang, X.; Zhou, D.; Li, P.; Guo, X.; Sun, B.; Liu, H.; Yan, K.; Gogotsi, Y.; Wang, G. MXene-Based Dendrite-Free Potassium Metal Batteries. *Adv. Mater.* **2020**, *32*, 1906739.

(38) Zhang, X.; Lv, R.; Wang, A.; Guo, W.; Liu, X.; Luo, J. MXene Aerogel Scaffolds for High-Rate Lithium Metal Anodes. *Angew. Chem., Int. Ed.* **2018**, *57*, 15028−15033.

(39) Fang, Y.; Zhang, Y.; Zhu, K.; Lian, R.; Gao, Y.; Yin, J.; Ye, K.; Cheng, K.; Yan, J.; Wang, G. Lithiophilic Three-Dimensional Porous $Ti_3C_2T_x$-rGO Membrane as a Stable Scaffold for Safe Alkali Metal (Li or Na) Anodes. *ACS Nano* **2019**, *13*, 14319.

(40) Zhang, C.; Kremer, M. P.; Seral-Ascaso, A.; Park, S. H.; McEvoy, N.; Anasori, B.; Gogotsi, Y.; Nicolosi, V. Stamping of Flexible, Coplanar Micro-Supercapacitors Using MXene Inks. *Adv. Funct. Mater.* **2018**, *28*, 1705506.

(41) Xu, H.; Yin, X.; Li, X.; Li, M.; Liang, S.; Zhang, L.; Cheng, L. Lightweight Ti_2CT_x MXene/Poly (Vinyl Alcohol) Composite Foams for Electromagnetic Wave Shielding with Absorption-Dominated Feature. *ACS Appl. Mater. Interfaces* **2019**, *11*, 10198−10207.

(42) Fan, L.; Zhuang, H. L.; Zhang, W.; Fu, Y.; Liao, Z.; Lu, Y. Stable Lithium Electrodeposition at Ultra-High Current Densities Enabled by 3D PMF/Li Composite Anode. *Adv. Energy Mater.* **2018**, *8*, 1703360.

(43) Wang, N.-N.; Wang, H.; Wang, Y.-Y.; Wei, Y.-H.; Si, J.-Y.; Yuen, A. C. Y.; Xie, J.-S.; Yu, B.; Zhu, S.-E.; Lu, H.-D. Robust, Lightweight, Hydrophobic, and Fire-Retarded Polyimide/MXene Aerogels for Effective Oil/Water Separation. *ACS Appl. Mater. Interfaces* **2019**, *11*, 40512−40523.

(44) Yan, J.; Ren, C. E.; Maleski, K.; Hatter, C. B.; Anasori, B.; Urbankowski, P.; Sarycheva, A.; Gogotsi, Y. Flexible MXene/

Graphene Films for Ultrafast Supercapacitors with Outstanding Volumetric Capacitance. *Adv. Funct. Mater.* **2017**, *27*, 1701264.

(45) Jin, S.; Sun, Z.; Guo, Y.; Qi, Z.; Guo, C.; Kong, X.; Zhu, Y.; Ji, H. High Areal Capacity and Lithium Utilization in Anodes Made of Covalently Connected Graphite Microtubes. *Adv. Mater.* **2017**, *29*, 1700783.

(46) Xue, P.; Liu, S.; Shi, X.; Sun, C.; Lai, C.; Zhou, Y.; Sui, D.; Chen, Y.; Liang, J. A Hierarchical Silver-Nanowire-Graphene Host Enabling Ultrahigh Rates and Superior Long-Term Cycling of Lithium-Metal Composite Anodes. *Adv. Mater.* **2018**, *30*, 1804165.

(47) Zhang, R.; Chen, X. R.; Chen, X.; Cheng, X. B.; Zhang, X. Q.; Yan, C.; Zhang, Q. Lithiophilic Sites in Doped Graphene Guide Uniform Lithium Nucleation for Dendrite-Free Lithium Metal Anodes. *Angew. Chem., Int. Ed.* **2017**, *56*, 7764−7768.

(48) Liu, W.; Xia, Y.; Wang, W.; Wang, Y.; Jin, J.; Chen, Y.; Paek, E.; Mitlin, D. Pristine or Highly Defective? Understanding the Role of Graphene Structure for Stable Lithium Metal Plating. *Adv. Energy Mater.* **2019**, *9*, 1802918.

(49) Tian, Y.; An, Y.; Wei, C.; Xi, B.; Xiong, S.; Feng, J.; Qian, Y. Flexible and Free-Standing $Ti_3C_2T_x$ MXene@ Zn Paper for Dendrite-Free Aqueous Zinc Metal Batteries and Nonaqueous Lithium Metal Batteries. *ACS Nano* **2019**, *13*, 11676−11685.

(50) Shi, H.; Zhao, X.; Wu, Z.-S.; Dong, Y.; Lu, P.; Chen, J.; Ren, W.; Cheng, H.-M.; Bao, X. Free-Standing Integrated Cathode Derived from 3D Graphene/Carbon Nanotube Aerogels Serving as Binder-Free Sulfur Host and Interlayer for Ultrahigh Volumetric-Energy-Density Lithium Sulfur Batteries. *Nano Energy* **2019**, *60*, 743−751.

(51) Li, G.; Liu, Z.; Huang, Q.; Gao, Y.; Regula, M.; Wang, D.; Chen, L.-Q.; Wang, D. Stable Metal Battery Anodes Enabled by Polyethylenimine Sponge Hosts by Way of Electrokinetic Effects. *Nat. Energy* **2018**, *3*, 1076−1083.

(52) Wang, C.; Wang, H.; Matios, E.; Hu, X.; Li, W. A Chemically Engineered Porous Copper Matrix with Cylindrical Core-Shell Skeleton as a Stable Host for Metallic Sodium Anodes. *Adv. Funct. Mater.* **2018**, *28*, 1802282.

(53) Wang, A.; Hu, X.; Tang, H.; Zhang, C.; Liu, S.; Yang, Y. W.; Yang, Q. H.; Luo, J. Processable and Moldable Sodium-Metal Anodes. *Angew. Chem., Int. Ed.* **2017**, *56*, 11921−11926.

(54) Luo, J.; Wang, C.; Wang, H.; Hu, X.; Matios, E.; Lu, X.; Zhang, W.; Tao, X.; Li, W. Pillared MXene with Ultralarge Interlayer Spacing as a Stable Matrix for High Performance Sodium Metal Anodes. *Adv. Funct. Mater.* **2019**, *29*, 1805946.

(55) Zhou, F.; Huang, H.; Xiao, C.; Zheng, S.; Shi, X.; Qin, J.; Fu, Q.; Bao, X.; Feng, X.; Müllen, K. Electrochemically Scalable Production of Fluorine-Modified Graphene for Flexible and High-Energy Ionogel-Based Microsupercapacitors. *J. Am. Chem. Soc.* **2018**, *140*, 8198−8205.

(56) Zhao, M. Q.; Ren, C. E.; Ling, Z.; Lukatskaya, M. R.; Zhang, C.; Van Aken, K. L.; Barsoum, M. W.; Gogotsi, Y. Flexible MXene/Carbon Nanotube Composite Paper with High Volumetric Capacitance. *Adv. Mater.* **2015**, *27*, 339−345.

(57) Yao, Y.; Wei, Z.; Wang, H.; Huang, H.; Jiang, Y.; Wu, X.; Yao, X.; Wu, Z.-S.; Yu, Y. Toward High Energy Density All Solid-State Sodium Batteries with Excellent Flexibility. *Adv. Energy Mater.* **2020**, *10*, 1903698.

(58) Delley, B. From Molecules to Solids with the $DMol^3$ Approach. *J. Chem. Phys.* **2000**, *113*, 7756−7764.

(59) White, J. A.; Bird, D. M. Implementation of Gradient-Corrected Exchange-Correlation Potentials in Car-Parrinello Total-Energy Calculations. *Phys. Rev. B: Condens. Matter Mater. Phys.* **1994**, *50*, 4954.

(60) Perdew, J. P.; Burke, K.; Ernzerhof, M. Generalized Gradient Approximation Made Simple. *Phys. Rev. Lett.* **1996**, *77*, 3865.

(61) Monkhorst, H. J.; Pack, J. D. Special Points for Brillouin-Zone Integrations. *Phys. Rev. B* **1976**, *13*, 5188.

(62) Xie, Y.; Naguib, M.; Mochalin, V. N.; Barsoum, M. W.; Gogotsi, Y.; Yu, X.; Nam, K. W.; Yang, X. Q.; Kolesnikov, A. I.; Kent, P. R. Role of Surface Structure on Li-Ion Energy Storage Capacity of Two-Dimensional Transition-Metal Carbides. *J. Am. Chem. Soc.* **2014**, *136*, 6385−6394.

(63) Cui, J.; Yao, S.; Ihsan-Ul-Haq, M.; Wu, J.; Kim, J.-K. Correlation between Li Plating Behavior and Surface Characteristics of Carbon Matrix toward Stable Li Metal Anodes. *Adv. Energy Mater.* **2019**, *9*, 1802777.